ISSN 1061-8309, Russian Journal of Nondestructive Testing, 2020, Vol. 56, No. 7, pp. 566–573. © Pleiades Publishing, Ltd., 2020.

ACOUSTIC METHODS

Performance Evaluation of Austenitic Stainless Steel Weld by Ultrasonic Phased Array Inspection Based on Probability of Detection

Qiang Wang[a], *, Kai Zhu[a], Linlin Wu[a], Haihang Li[a], Xiaomeng Xu[a], and Sifan Gong[a]

[a]*College of Quality and Safety Engineering, China Jiliang University, Hangzhou, Zhejiang, 310018 China*

**e-mail: qiangwang@cjlu.edu.cn*

Received March 30, 2019; revised December 14, 2019; accepted April 29, 2020

Abstract—To evaluation capability of ultrasonic phased array (PHA) in industrial austenitic stainless steel (ASS) weld quantitatively, the 304 ASS butted weld specimen with various depth and side-drilled holes (SDH) was drilled to analyze reliability of PHA testing. Based on phased array probes, the ultrasonic waveform data are processed by in traditional dynamic depth focusing and total focusing method (TFM). The welding zone defects imaging results are compared. The probability of detection (POD) curves of ultrasonic response data were used for estimation the detection capability and reliability of ultrasonic PHA.

Keywords: ultrasonic phased array, austenitic stainless steel, weld, microstructure, probability of detection

DOI: 10.1134/S1061830920070086

1. INTRODUCTION

Due to the excellent ductility and relatively low yield strength of austenitic stainless steel (ASS), strain strengthening technology is used for pressure equipments in nuclear power plant, such as auxiliary circuits of nuclear power plant are austenitic stainless steel. The non-destructive testing (NDT) techniques must allow the detection of the potential defects in the stainless steel pipes and welding [1, 2]. Though the ultrasonic examination was often used to inspect overlaying weld defects of large-scale steel structure made of alloy Cr5 cast steel or carbon steel [3], while the ASS welding zone is a difficult component to test using ultrasonic test, due to anisotropic nature of the welding zone and columnar grain size [4]. Attenuation of high frequency ultrasound, backscattering noise and beam redirection in ASS weld materials cause difficulties in the ultrasonic testing. Inspection of coarse-grained welding zone using ultrasonic phased array (PHA) has a relatively low probability of detection of cracks, because the crystalline structure of welds causes distortion and splitting of the ultrasonic beams which propagates anisotropic medium [5].

The manufacturing flaws, such as voids, un-fusions and cracks exist in ASS welded joints. Inspection of austenitic welds was carried out mainly on radiographic techniques [6]. The developed ultrasonic phased array system and flaw classification concept are expected to enhance the efficiency and reliability of the NDT of nuclear power plant components [7]. The focusing effect of the PHA can improve the signal-to-noise ratio (SNR) in coarse grained material. The combination of mechanical scanning and electronic beam steering increases the flaw detect-ability. Concerning the flaw detection in highly scattering environment, it also was used to actual polycrystalline weld materials (a nickel-based alloy) defects detection [8]. A procedure for generating probability of detection (POD) based on ultrasonic simulation synthetic data were developed [9]. It specifies ultrasonic inspection of piping components within Swedish nuclear power plants.

The POD has been used as a quantitative measurement to evaluate the detection capability and reliability of a NDT&E technique [10, 11]. The POD is strongly connected to the topic risk assessment and probabilistic analysis in the evaluation of the performance of components including the nuclear components, and it provides the probability for the detection of certain flaw size in coarse-grain structure. After synthetic aperture focusing technique (SAFT) processing, the ultrasonic data acquired on a test block (coarse grain material) with model defects an $\hat{a}$ vs. a approach has been performed to determine the POD for the inspected duplex specimen [12]. The total focus method (TFM) and phase-coherent imaging have

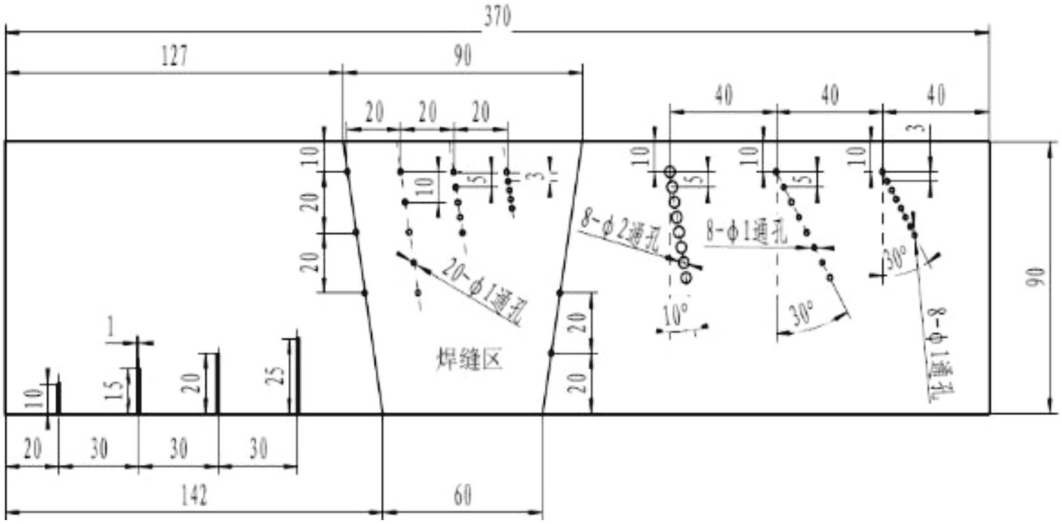

Fig. 1. ASS specimen with butted weld (side drilled holes).

been proposed to consider the statistics of detection, presenting the detection performance as POD, the detection performance of different imaging algorithms on a coarse-grained power plant material [13]. The detection of real and artificial flaws of different sizes and different types using ultrasound is considered. The POD provides the probability for the detection of a certain flaw size [14]. The experimental POD determination from inspections of test blocks with real cracks in austenitic test specimen was presented [16].

In this paper, we focus on the influence of various defect depths on the reliability of ultrasonic PHA inspection of industrial 304 ASS weld in mock-up. The 5 MHz phased array probes performances are compared with Φ 1 mm side-drilled flaws detection in welding zone. Traditional sectional scan imaging and TFM imaging results are compared. Finally, the detection performance is evaluated by utilizing POD model based on experimental data.

2. SPECIMEN OF 304 ASS

The 304 ASS specimen with butted weld is machined to evaluate the reliability of phased array POD for reference defects. The sketch and physical map of type-304 ASS blocks joined by butt weld are illustrated in Fig. 1. The block size is 370 mm × 90 mm × 30 mm. And typical side drilled holes (SDH Φ 1 mm) and other artificial cutting flaws are machined in the weld zone. Also these defects distributed in wedge welding zone and fusion zone in block.

Though extensive metallographic investigations on microstructure of the ASS weld material were conducted [17], we also analyzed the metallographic pictures 304 ASS block (370 mm × 90 mm × 10 mm). The 6 slice of the block (10 mm × 10 mm × 10 mm) were extracted from specimen. The micrograph of specimen in weld zone and fusion zone were polished and corroded by hydrochloric acid liquid. The photographs of specimen microstructure are shown in Fig. 2.

The 304 ASS weld anisotropy causes a steering of the ultrasonic beam leading to a number of adverse effects upon ultrasonic array imagery, including defect mislocation and aberration of the defect response. In Fig. 2a, the polycrystalline structure is observed which will cause the beam distortion. The 304 ASS welding area average grain size is around 419.4 μm, which is the several times than the grain size in base metal. Two sets of five Φ1 mm SDH (depth 10, 20, 30, 40, 50 mm) and Φ1 mm SDH (depth 10, 15, 20, 25, 30 mm) are machined in this zone. In Fig. 2b, there exists obvious fusion line in fusion zone and three typical Φ1 mm SDH (depth 10, 30 and 50 mm) in this area. The fusion line width is about 149.1 μm. The grains distribution at the left of fusion line near the weld region is coarse in shape and owns prominent cylindrical crystal in different directions. The right side of fusion line near base material zone is heat-affected zone.

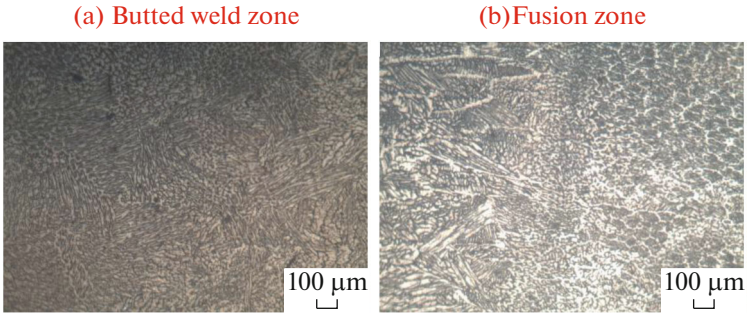

Fig. 2. Metallographic pictures of ASS specimen with butted weld.

3. ULTRASONIC INSPECTIONS DATA

3.1. Traditional Sectional Scan Images

The coarse-grained 304 ASS weld zone defects were tested on the experimental data. We focus on the mock-up contains three sets of five Φ 1 mm SDHs with different depth. Set 1, five Φ 1 mm SDHs with depth 10, 15, 20, 25 and 30 mm in welding zone, set 2, five Φ 1 mm SDHs with depth 10, 20, 30, 40 and 50 mm in welding zone and set 3, three Φ 1 mm SDHs with depth 10, 30 and 50 mm in fusion zone. The OmniScan MX2 ultrasonic phased array system and 5 MHz probe are used in test. The sector-scan views corresponding to beam steering 30° to 70° are presented in Fig. 3. For 5 MHz probe, the SNR of 10, 15, 20, 25 and 30 mm SDHs are 20.3, 18.8, 15.6, 14.1, and 12.5 dB.

In Fig. 3a, the five Φ 1 mm SDHs with space 5 mm with dynamic focusing is presented. In the 30 mm, the SNR decreases to 12.5 dB. Though we are able to discern the five defects, the accurate holes' positions are not easy to be determined. In Fig. 3b, just three SDHs (depth 10, 20, 30 mm) are inspected in approximate position, while the SDHs (depth 40 mm and depth 50 mm) are covered by strong structure noise of coarse grains. It is observed that traditional dynamic focusing method cannot detect flaws depth more than 30 mm in ASS welding zone. In Fig. 3c, three SDHs are correctly detected in fusion zone owing to the ultrasonic waveform propagating through the base metal area and reached the fusion zone. The probe position is on the left of set 3 holes top surface.

The Φ 1 mm SDH are along the full width at depths 10 to 50 mm are imaged with PHA. The left images in Fig. 4 are defects ultrasonic data in base metal zone and the right images are the same sizes defects signals in weld zone. It is clear that strong structural noise occurs in weld zone for the 50 mm depth defects detection compared with detection in base metal zone.

Quantitative contrast was displayed in Table 1. For the same defect size and depth, there exists about 10 dB gain difference between welding zone and base metal zone. The SNR reduces about 12 dB owing to acoustic wave attenuates in welding zone.

3.2. TFM Images

The full matrices capture by positioning channel right above the each flaw with (64 elements probe) of CTS-PA22T (Shantou Institute of Ultrasonic Instruments Co.) phased array system. The advantages of this system allow to recorder the full data set of all acoustic responses between emitter and receiver. The total focus method (TFM) algorithm is applied to the full matrix data [15]. All flaws in block are well detected by the TFM. With the TFM, imaging is restricted to the (x, z) plane covered by the array probe

Table 1. Contrast Φ1 SDHs in weld zone with varied depths

Depths, mm	Weld zone	
	dB value (80% amplitude)	SNR, dB
10	53	20.3
20	57	16.5
30	63	10.1
40	67	8.6
50	72	6.4

(a) set 1 SDH image

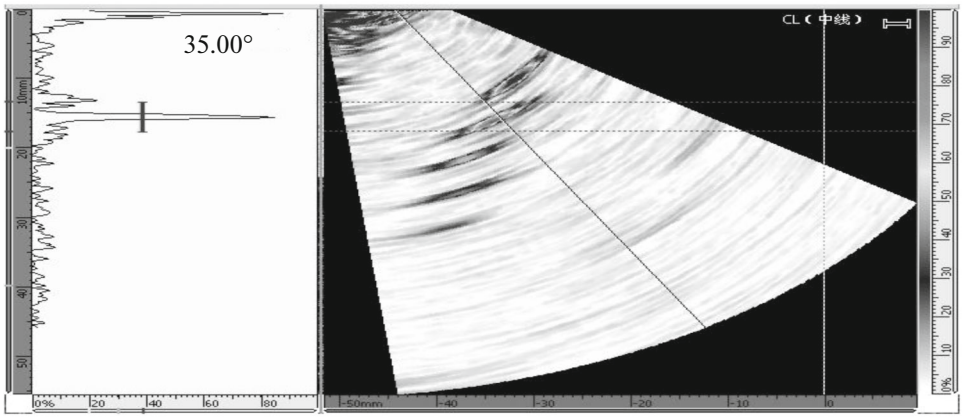

(b) set 2 SDH image

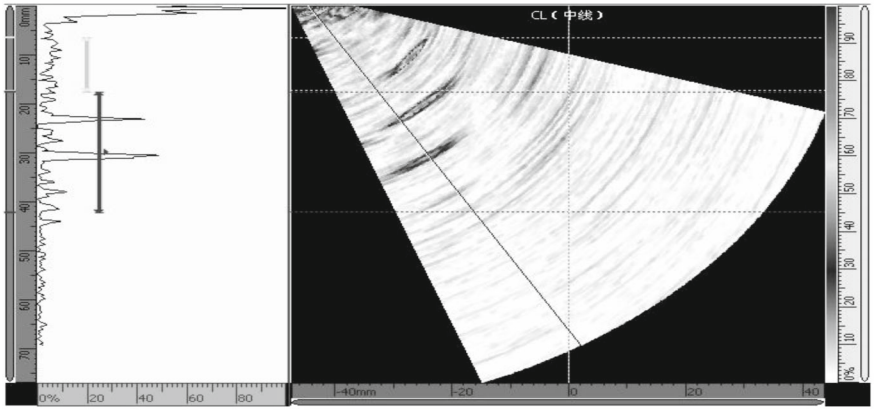

(c) set 3 SDH image

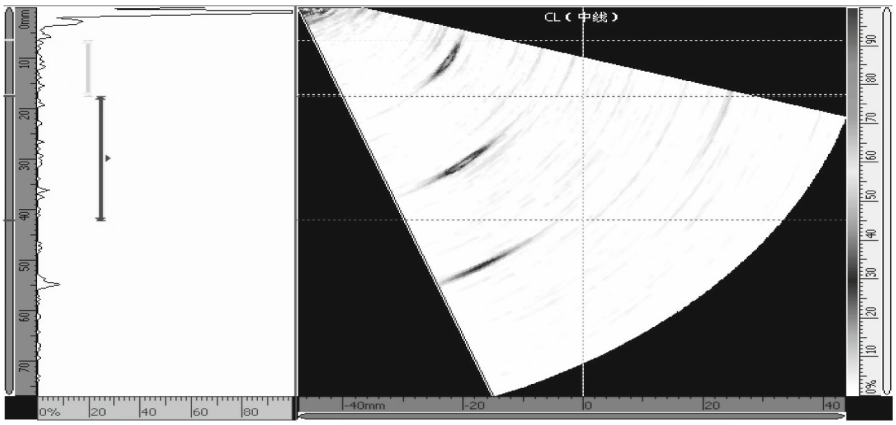

Fig. 3. Images for the SDH at different depths in fusion and welding zone.

(5 MHz, longitudinal wave). The shadow of the defect with the largest depth (50 mm) in Figs. 5b and 5c are also well observed. It is easy to capture the flaw position. Therefore, the TFM is able to image nearly perfectly all SDHs in ASS block butt welding zone and provides good response. It provides a synthetic image of high quality in ASS welding zone and fusion zone. It improved the SNR, compared with images in Fig. 3.

4. POD ANALYSIS

To quantitatively analyze reliability of ultrasound phased array detection in base metal zone and weld zone, the POD was calculated based on ultrasonic signal response. The POD allows quantifying the reli-

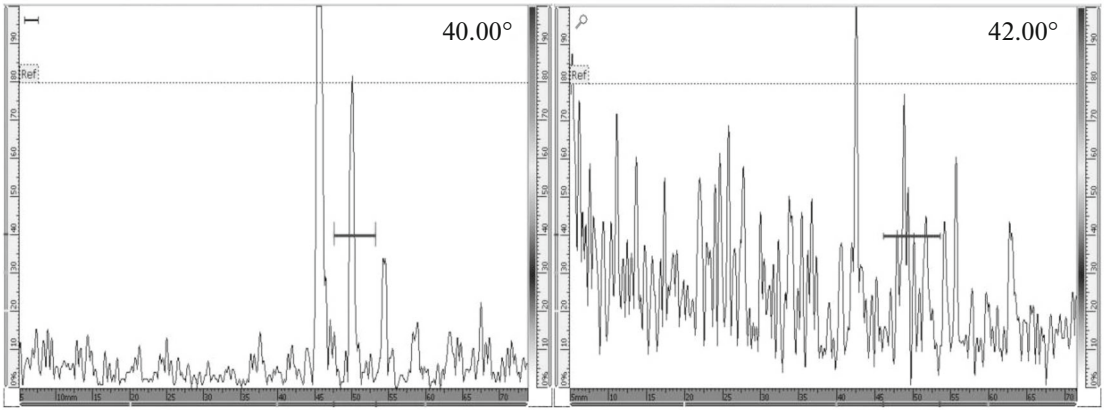

Fig. 4. Ultrasonic detection signal of defects with 50 mm depth.

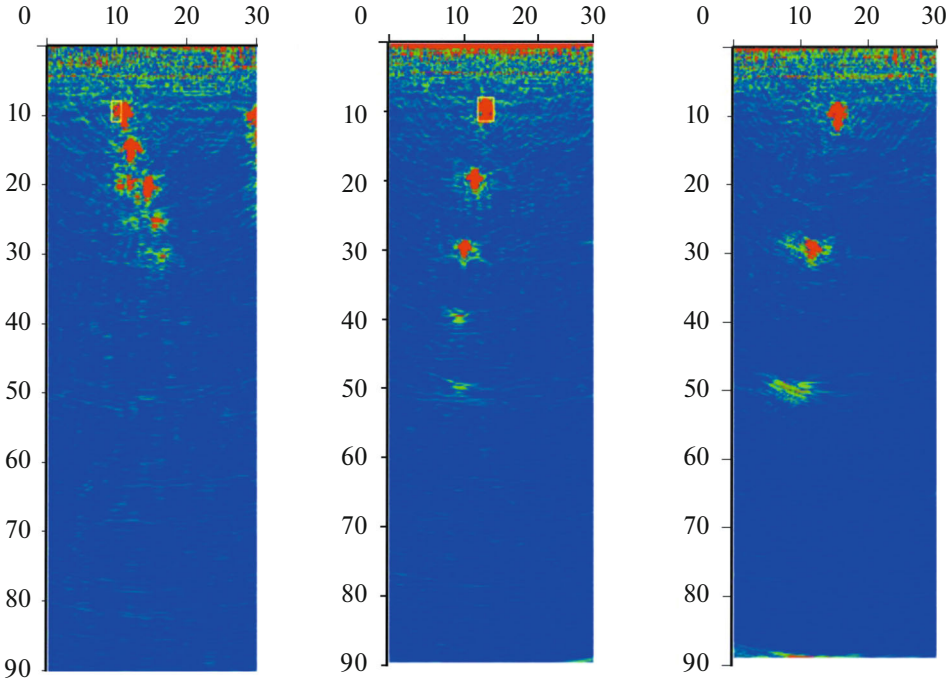

(a) set 1 five Φ 1 mm SDHs (b) set 2 five Φ 1 mm SDHs (c) set 3 three Φ 1 mm SDHs

Fig. 5. Total focusing method images of SDHs in welding zone and fusion zone.

ability of PHA method for austenitic specimen. Based on the correlation of signal response and flaw size ($\hat{a}$ vs. a), the POD determination method was carried out for ultrasonic wave data [17]. A critical point in the POD analysis of signal response data is the decision threshold $\hat{a}_T$. If the ultrasonic wave response value $\hat{a}$ is larger than $\hat{a}_T$, it will be regarded as a flaw. There are two indications a_{90} and $a_{90/95}$ are used to analyze the POD. ($a_{90/95}$ represents the values of the flaw depth with 90% POD within a confidence interval of 95%), and a_{90} means that the depth of flaw detected is a when the detection probability is 90% [18].

Based on the classical signal response model, we regard the signal response value $\hat{a}$ also has relation with the defect depth a [11].

$$\hat{a} = \beta_0 + \beta_1 \log(a) + \delta, \tag{1}$$

where δ is random error is normally distributed $(0, \sigma_\delta^2)$, β_0, β_1 and δ are the regression parameters associated with the signals. If $\hat{a} > \hat{a}_T$, the POD can be determined, for each defect,

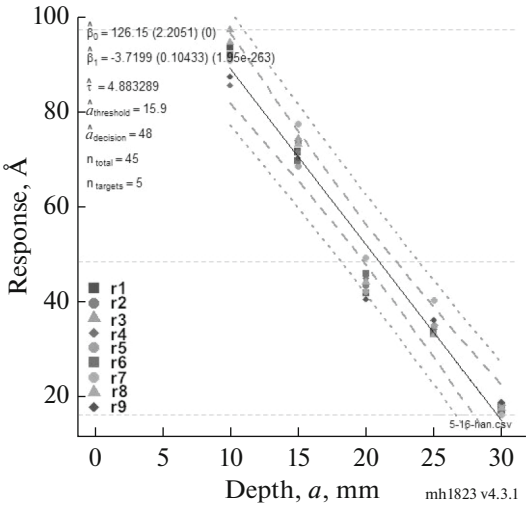

Fig. 6. Linear model of signal response data in Welding zone.

$$\mathrm{POD}(a) = P(\hat{a} > \hat{a}_T) = P(\delta > \hat{a}_T - \beta_0 - \beta_1 \log(a)), \tag{2}$$

$$\mathrm{POD}(a) = 1 - \Phi\left\{\frac{\hat{a}_T - (\beta_0 + \beta_1 a)}{\sigma_\delta}\right\}, \tag{3}$$

where Φ is the cumulative distribution of normal distribution with mean μ and standard deviation σ_δ, then the POD determination is written as,

$$\mathrm{POD}(a) = \Phi\left\{\frac{\ln a - \mu}{\sigma}\right\}, \tag{4}$$

then $\mu = \dfrac{\hat{\alpha}_T - \beta_0}{\beta_1}$, $\sigma = \dfrac{\sigma_\delta}{\beta_1}$, β_0, β_1 and σ_δ are calculated by maximum likelihood estimation of linear regression over signal responses collected for a range of flaw depths.

The ultrasonic PHA inspections are conducted on artificial SDHs of various depths whose diameter is 1 mm and interval is 5 mm. As shown in Fig. 1, these artificial defects distributed in welding zone. For each flaw of the same depth, we gathered 30 groups of data that meet signal response model. Then, a series of signal response amplitudes of varied depths are obtained, these data are processed by mh1823POD software [19]. The linear model of signal response data are presented in Fig. 5, where the black line means linear fitting curve, the most outside dashed lines represents the prediction range with 95% confidence, the two dotted lines near the black line represents the confidence interval with 95% confidence, and r1–r9 means 9 response signal per SDH test for welding zone.

In Fig. 6, the linear model agrees with the experimental data, and is suitable to calculate POD. Based on comparison data, the signal response value $\hat{a}$ in base metal material is large than in weld zone for the same depth of defect. When defects depth varies from 10 to 30 mm, the difference value of $\hat{a}$ is about 50 in base metal zone and 70 in weld zone. The regression variance $\hat{\tau}$ of linear regression model in base metal zone is 3.64, while $\hat{\tau}$ is 4.88 in weld zone. It is obvious that $\hat{a}$ deviation of the linear regression model is different in base metal and welding zones. The response threshold $\hat{a}_T$ is determined as half the value of signal maximum amplitude. The POD curves of detection results in the two zones are gained by mh1823POD software.

From POD curves in Fig. 7, then $a_{90} = 19.33$ and $a_{90/95} = 20.65$ in weld zone, the detectable depth of defect is 19.33 mm when the detection rate is 90%. When the confidence is 95%, the detectable depth is 20.65 mm with 90% detection rate.

5. CONCLUSIONS

The 304 ASS block with SDHs in butted weld zone and fusion zone were design to evaluate the PHA detection performance. The PHA ultrasonic images of flaws (Φ 1 mm) in fusion zone and weld zones are

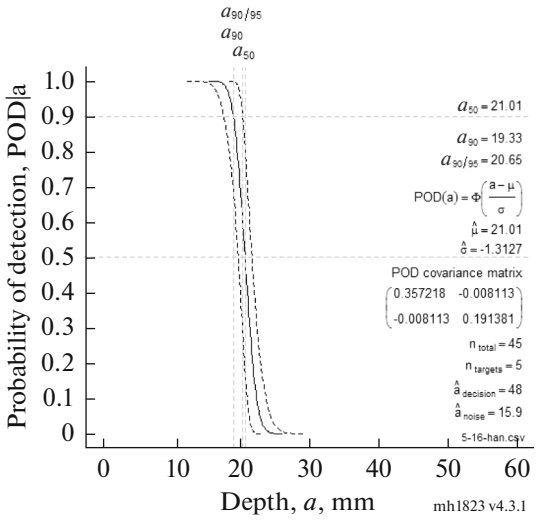

Fig. 7. POD curve in welding zone.

compared with TFM and traditional dynamic focusing. The inspection results from the 304 ASS specimens were discussed in form of $\hat{a}$ vs. a POD analysis. From POD calculation, it means 304 ASS weld reduces flaw detection capability due to structural noise.

FUNDING

This work was supported by National Key R&D Program of China under grant 2018YFC0808500.

REFERENCES

1. Bolotina, I., Dyakina, M., Kröning, M., Mohr, F., Reddy, K.M., Soldatov, A., and Zhantlessov, Y., Ultrasonic arrays for quantitative nondestructive testing an engineering approach, *Russ. J. Nondestr. Test.,* 2013, vol. 49, no. 3, pp. 145–158.
2. Wafik Harara and Ahmad Altahan, Attempt towards the replacement of radiography with phased array ultrasonic testing of steel plate welded joints performed on bridges and other applications, *Russ. J. Nondestr. Test.,* 2018, vol. 54, no. 5, pp. 335–344.
3. Qingbao Wang, Zhuoxin Li, Yaowu Shi, Lizhi Wang, and Fei Liu, Interior crack and its formation mechanism in overlaying weld of back-up rolls, *Eng. Failure Anal.*, 2013, vol. 34, pp. 268–277.
4. Chassignole, B., Duwig, V., Ploix, M.-A., Guy, P., and El Guerjouma, R., Modelling the attenuation in the ATHENA finite elements code for the ultrasonic testing of austenitic stainless steel welds, *Ultrasonics*, 2009, vol. 49, no. 8, pp. 653–658.
5. Nowers, O., Duxbury, D.J., and Drinkwater, B.W., Ultrasonic array imaging through an anisotropic austenitic steel weld using an efficient ray-tracing algorithm, *NDT&E Int.,* 2016, vol. 79, pp. 98–108.
6. Casalta, S., Daquino, G.G., Metten, L., Oudaert, J., and Van de Sande, A., Digital image analysis of X-ray and neutron radiography for the inspection and the monitoring of nuclear materials, *NDT&E Int.,* 2003, vol. 36, no. 5, pp. 349–355.
7. Sung-Jin Song, Hyeon Jae Shin, and You Hyun Jang, Development of an ultrasonic phased array system for nondestructive tests of nuclear power plant components, *Nucl. Eng. Des.*, 2002, vol. 214, pp. 151–161.
8. Shahjahan, S., Rupin, F., Aubry, A., Chassignole, B., Fouquet, T., and Derode, A., Comparison between experimental and 2-D numerical studies of multiple scattering in Inconel600® by means of array probes, *Ultrasonics*, 2014, vol. 54, no. 1, pp. 358–367.
9. Wirdelius, H. and Persson, G., Simulation based validation of the detection capacity of an ultrasonic inspection procedure, *Int. J. Fatigue*, 2012, vol. 41, pp. 23–29.
10. Pilyugin, S.O. and Lunin, V.P., Determining the probability of detecting flaws in weld joints by phased-array ultrasonic testing, *Russ. J. Nondestr. Test.,* 2016, vol. 52, no. 6, pp. 332–338.
11. Berens, A.P., NDE reliability data analysis quantitative nondestructive evaluation, in *ASM Metals Handbook,* 1976, vol. 17, pp. 689–701, 8th ed.

12. Spies, M. and Rieder, H., Synthetic aperture focusing of ultrasonic inspection data to enhance the probability of detection of defects in strongly attenuating materials, *NDT&E Int.,* 2010, vol. 43, no. 5, pp. 425–431.
13. Van Pamel, A., Brett, C.R., and Lowe, M.J.S., A methodology for evaluating detection performance of ultrasonic array imaging algorithms for coarse-grained materials, *IEEE Trans. Ultrason. Eng.*, 2014, vol. 61, no. 12, pp. 2042–2053.
14. Yusa, N., Chen, W., and Hashizume, H., Demonstration of probability of detection takingconsideration of both the length and the depth of a flaw explicitly, *NDT&E Int.,* 2016, vol. 81, pp. 1–8.
15. Holmes, C., Drinkwater, B.W., and Wilcox, P.D., Post-processing of the full matrix of ultrasonic transmit–receive array data for non-destructive evaluation, *NDT&E Int.,* 2005, vol. 38, no. 8, pp. 701–711.
16. Kurz, J.H., Jüngert, A., Dugan, S., et al., Reliability considerations of NDT by probability of detection (POD) determination using ultrasound phased array, *Eng. Failure Anal.*, 2013, vol. 35, no. 26, pp. 609–617.
17. Nageswaran, C., Carpentier, C., and Tse, Y.Y., Microstructural quantification, modelling and array ultrasonics to improve the inspection of austenitic welds, *Insight*, 2009, vol. 51, no. 12, pp. 660–666.
18. Demeyer, S., Jenson, F., Dominguez, N., and Iakovleva, E., Transfer function approachbased on simulation results for the determination of pod curves, in *Rev. Progr. Quant. Nondestr. Eval. AIP Conf. Proc.,* Thompson, D.O. and Chimenti, D.E., Eds., Burlington, VT, 2012, pp. 1757–1764.
19. Annis, C., *MIL-HDBK-1823A. Nondestructive Evaluation System Reliability Assessment. Department of Defense Handbook,* USA: Wright-Patterson AFB, 2009.